INVESTIGATION OF SKIN-CORE DEBONDING IN SANDWICH PANEL STRUCTURES WITH PMI FOAM CORES

G. Bragagnolo[1,2], A. D. Crocombe[1], S. L. Ogin[1], I. Mohagheghian[1], A. Sordon[2], G. Meeks[2]

[1]Department of Mechanical Engineering Sciences, University of Surrey, Guildford, UK
Email: g.bragagnolo@surrey.ac.uk; a.crocombe@surrey.ac.uk; s.ogin@surrey.ac.uk;
i.mohagheghian@surrey.ac.uk
Web Page: http://www.surrey.ac.uk/mes/index.htm
[2]McLaren Automotive Ltd., Woking, Surrey, UK
Email: alessandro.sordon@mclaren.com; graham.meeks@mclaren.com

Keywords: Sandwich structures; Foam core; Debonding; FEA; Skin-core interface

Abstract
Skin-core debonding in sandwich specimens with CFRP skins and a PMI foam core has been investigated. Mode I and Mode II tests have been carried out to analyse the skin-core interface response when different foam types are used as core material, and the Digital Image Correlation (DIC) technique, has been used to provide full-field strain information. The results show that foams with a large cell size favour a high resin uptake at the interface during the manufacturing process, which allows a better bonding to the composite skin. Finite element analysis with the cohesive zone method and a crushable foam model has been used to simulate the structural response; the numerical predictions are in good agreement with the experimental results. Furthermore, the importance of including the resin layer at the interface within the numerical modelling is discussed.

1. Introduction

Sandwich composite structures can absorb a large amount of energy during impact; this is one of the reasons why such materials are used in crashworthy applications. The choice of the materials used for the core and skin of the sandwich panel plays an extremely important role in the structural response and in the skin-core interfacial behaviour. The debonding phenomenon between composite skins and foam core, which is one of the major failure modes during a crush event, has been investigated experimentally, analytically and numerically [1-5]. However, while PVC foams have been thoroughly characterised, research on PMI foams for sandwich structure applications is still ongoing [5-7].

In this work, three close-celled PMI foam types are considered as core materials. They differ in density, cell size and manufacturing process. A Vacuum Assisted Resin Transfer Moulding (VARTM) technique was used to manufacture sandwich specimens with carbon fibre skins and a PMI foam core. Double Cantilever Beam (DCB) and Cracked Sandwich Beam (CSB) test configurations, defined by Carlsson [8], have been considered with the aim of characterising the skin-core interface and extracting the Mode I and Mode II critical energy release rates. The effect of foam cell size on the interface performance has been examined and DIC has been used to obtain full-field strain information for specimens under CSB loading and to capture the strain concentration at the crack tip. The experimental results for both test configurations are compared to the Finite Element (FE) model predictions.

2. Experimental Methods

Symmetric sandwich panels with dimensions of 230 × 170 × 18 mm were made using VARTM technique. After curing, the panels were cut using a water jet cutter to obtain samples with the dimensions specified in Table 2 for DCB and CSB tests. Three close-celled PMI foam types were considered as core material. Figure 1 shows the microstructure of these foams while Table 1 summarises their most relevant macroscopic material properties. Young's modulus and tensile and compressive strength were taken from a study by Carranza Guisado [9] while the Mode I critical energy release rate was determined by single-edge-notch bending (SENB) test defined in the ASTM D5045 standard [10]. Carbon non-crimp fabric (NCF) +45/-45 432 g/m^2 biaxial material was used to manufacture the sandwich face sheets. A 12 μm-thick and 50 mm-long PTFE tape was inserted between the top skin and the core prior to the infusion process in order to create an initial crack. The layup of the overall panel was: 0/45/90/PMI foam/90/45/0.

Table 1. Foam core geometric and mechanical properties.

	Foam (a)	Foam (b)	Foam (c)
Average cell size [μm]	400	45	50
Young's modulus [MPa]	92	90	143
Tensile strength [MPa]	2.5	1.3	1.9
Compressive strength [MPa]	1.3	1.3	1.9
Critical strain energy release rate [kJ/m^2]	0.145	0.089	0.108

Mode I and Mode II test configurations are shown schematically in Figure 2 and Figure 3 respectively. Both tests have been loaded in displacement control with a constant rate of 1 mm/min for the DCB test and 0.5 mm/min for the CSB test. The surface of the samples containing the crack were painted white and a scale was drawn to monitor the crack growth. A video microscope was also used to help identify the position of the crack during propagation. However, the exact detection of the crack tip was difficult because of the porous nature of the foam that tended to obscure the crack tip. During Mode II testing, the DIC technique was used to obtain the full strain field of the specimen surface. The DIC system apparatus was supplied by Correlated Solutions Inc. and included two 9 megapixels cameras that were placed in front of the specimen during the test; Vic-3D software was used to analyse the images taken.

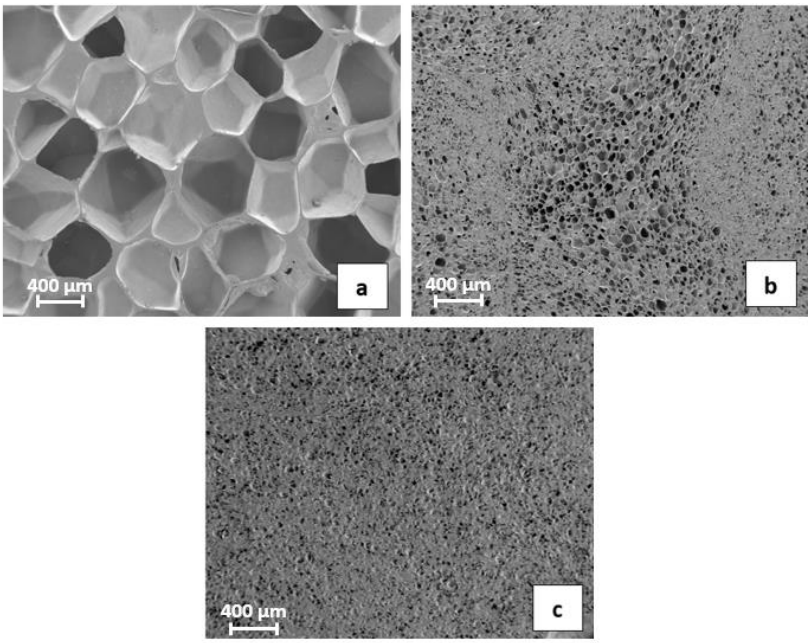

Figure 1. Scanning Electron Microscopy (SEM) micrographs of Foam (a), Foam (b) and Foam (c).

Figure 2. Schematic of the DCB specimen.

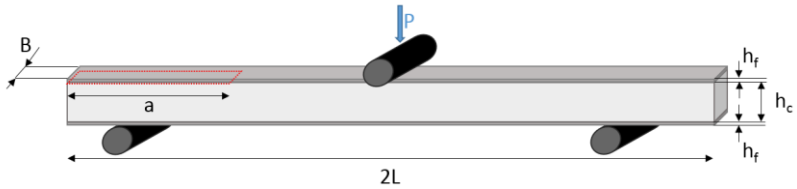

Figure 3. Schematic of the CSB specimen.

Table 2. Dimensions of DCB and CSB specimens.

	L [mm]	B [mm]	h_f [mm]	h_c [mm]	a [mm]
DCB	130	25	1.5	15	50
CSB	95	25	1.5	15	50

3. Numerical Analysis (FEA)

3D FE models were created using Abaqus to simulate the experimental tests. The geometry and dimensions of the modelled sandwich specimens are the same as those shown in Figure 2 and Figure 3. The entire sample was modelled as three different parts assembled and tied together: top skin, bottom skin and core. Skins and core were modelled using C3D8R (8-node linear brick) elements while zero thickness cohesive elements (COH3D8) were used to simulate the interfacial behavior between the top skin and the core during crack propagation. The skins were partitioned through the thickness to represent each composite ply, and ply orientations were specified according to the chosen layup. For DCB modelling, the loading was applied by displacement control to the edge of the top skin on the pre-cracked end of the sample, while all the degree of freedom at the bottom skin edge of the same end were fixed, so as to replicate the clamping condition of the experimental test. For the CSB test, the support rollers were modelled as discrete rigid bodies and a constant velocity was applied to the top roller. General contact was used to define the interaction between the specimen and the rollers, and to prevent penetration between different model parts. The whole model was meshed with a global element size of 1 mm.

A crushable foam model [11] with volumetric hardening was applied to the foam core, while the maximum nominal stress criterion (MAXS) and the power law failure criterion were used to define the damage initiation and evolution, respectively, of the cohesive elements. Table 3 summarises the properties used for the cohesive elements. t_n^0, t_s^0, t_t^0 are the maximum normal and two shear tractions respectively; they were estimated based on the foams' tensile and shear strengths. The critical energy release rate values were measured experimentally during DCB and CSB tests, as explained in the following sections.

Table 3. Cohesive elements material properties.

Foam type	G_{IC} [mJ/mm^2]	G_{IIC} [mJ/mm^2]	G_{IIIC} [mJ/mm^2]	t_n^0 [MPa]	t_s^0 [MPa]	t_t^0 [MPa]
Foam (a)	0.185	0.45	0.45	2.5	1.5	1.5
Foam (b)	0.1	1	1	1.3	1.5	1.5
Foam (c)	0.27	1	1	1.9	2.5	2.5

4. Results and Discussions

4.1. Experimental work

Load and displacement values were continuously recorded during testing. Figure 4 shows a comparison between the results of the three foam types considered. After the critical loading was reached, crack kinking occurred and the crack propagated inside the core parallel, and very close to, the face-core interface. The experimental curves present a slip-stick behaviour which is typical of brittle foams, with the first load peak corresponding to crack initiation. Composite sandwich samples with Foam (a) as core material showed a higher critical load for both Mode I and Mode II tests.

The interfacial behaviour depends on the foam cell size, resin and core ductility, core tensile strength and fracture toughness [12]. Foam (a) has a coarser cell size than the other two foams (as reported in Table 1). Therefore, the resin uptake at the interface is higher for Foam (a) than for Foam (b) and

Foam (c) and, as discussed in [13], low surface resin uptake in the fine-celled foams results in a lower surface bonding in sandwich panels where close-celled foam types are used as core material. Figure 5 shows images of the Foam (a) and Foam (b) skin-core interface taken with the optical microscope; the resin layer at the interface is notably thinner for the finer-celled foam.

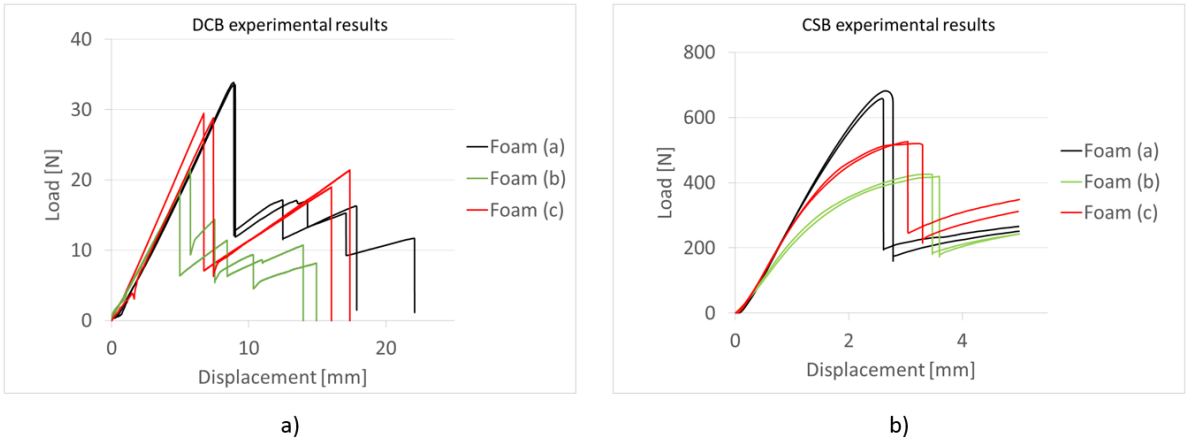

Figure 4. Experimental load-displacement curves: a) DCB results and b) CSB results.

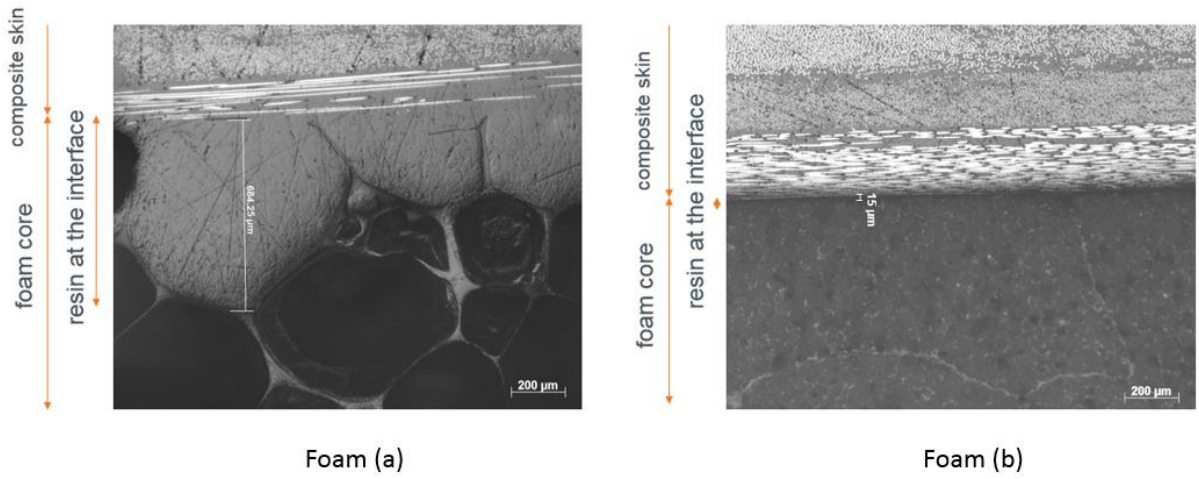

Figure 5. Micrographs of the skin-core interface of foam-cored sandwich specimens with Foam (a) and Foam (b) as core material.

4.2. Comparisons of experimental and finite element results

4.2.1 DCB test

G_{Ic} was computed using the beam theory [14] and its values at debonding initiation and at propagation are usually different because of the crack kinking phenomenon. There are contrasting views concerning the value of the critical energy release rate that should be considered as representative of the interface. The procedure used to produce the pre-crack (thickness and material of the insert) and the resin film at the interface (formed during the VARTM process when the resin enters the cells at the surface that have been cut open) are the cause of the initial higher value of G_{Ic}. For this reason,

Ramantani et al. [2] stated that the critical energy release rate calculated during propagation, after the initial micro-kinking at the crack tip, is the value that should be taken as representative of the interfacial fracture toughness. However, Rinker et al. [5] believe that the initiation value of G_{Ic} should be considered as the critical interfacial energy release rate because, after crack kinking, the G_{Ic} at propagation is more related to the foam fracture toughness than to the interfacial properties.

An example of the predicted load-displacement curves obtained using the measured $G_{Ic\ initiation}$ and $G_{Ic\ propagation}$ values as FEM input parameters is given for Foam (a) in Figure 6. When $G_{Ic\ initiation}$ is used to define the skin-core interfacial behaviour, the numerical curve accurately predicts crack initiation but overestimates the load peaks during propagation. The opposite happens when $G_{Ic\ propagation}$ is used as FEM input; the numerical curve underestimates the critical load for crack initiation but crack propagation is in good agreement with the experimental results.

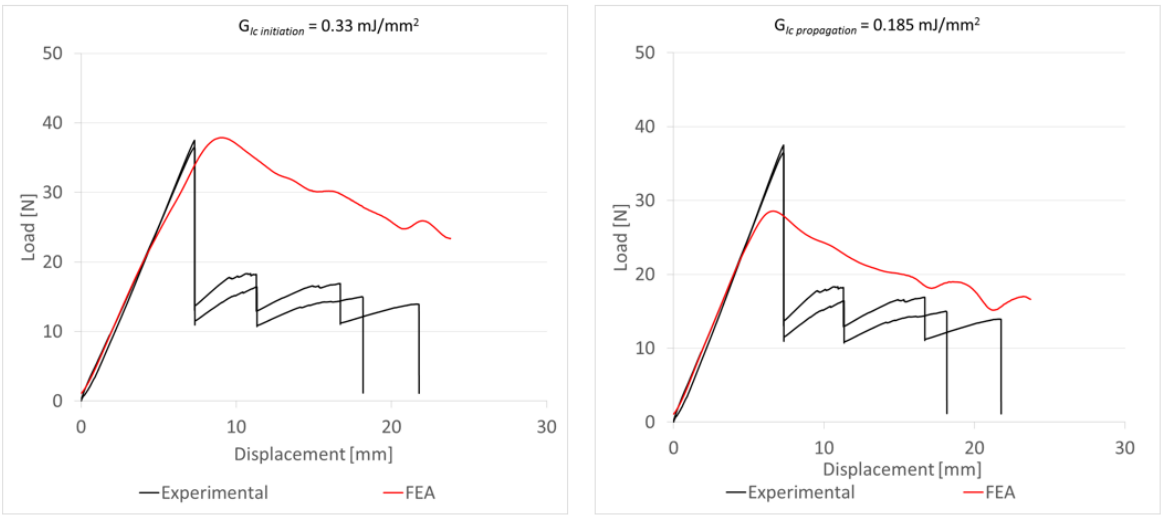

Figure 6. Comparison between numerical and experimental load-displacement curves using (a) G_{Ic} initiation and (b) G_{Ic} propagation as input for the FEM.

4.2.2 CSB test

Two different methods were employed to model CSB specimens. In the first method, a resin layer was added in the model between the cohesive elements and the foam core to represent the resin uptake at the interface where the foam cells were cut open (Figure 5). The second method omitted this thin resin layer and modelled only the cohesive elements between the skins and the foam core. In Figure 7, the full longitudinal strain field obtained with DIC, is compared to the numerical predictions of the longitudinal strain obtained with the two modelling methods for Foam (a). When the epoxy layer is included in the modelling, good agreement between the experimental and FE results is found. However, when the resin layer is neglected in the modelling, the compression of the foam under the crack tip is over-predicted. The results for Foam (b) are shown in Figure 8. Here, the strain is again over-predicted when the epoxy film at the interface is not modelled. However, the over-estimated strain is restricted to a much smaller area than in the Foam (a) FEA_No resin layer model. This is because of the much lower resin uptake at the interface and hence, thinner epoxy layer at the surface of the foam core.

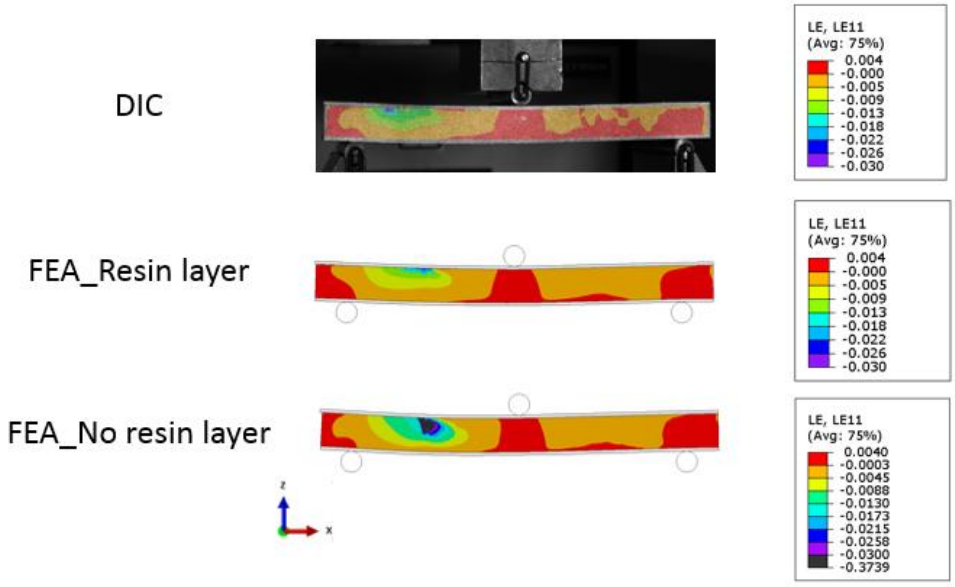

Figure 7. Comparison between DIC and FEA results for Foam (a). The full field of the longitudinal strain is considered.

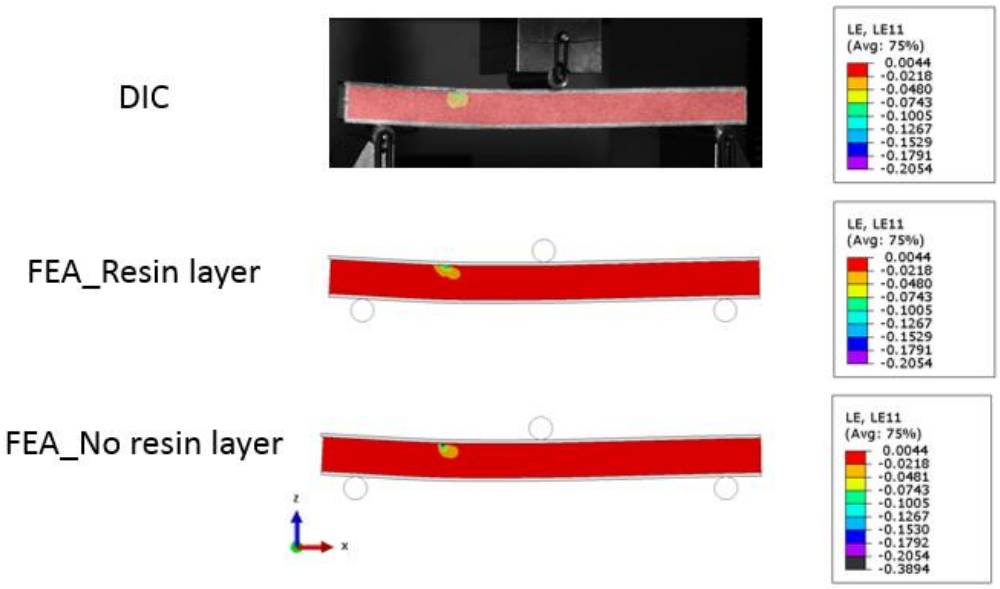

Figure 8. Comparison between DIC and FEA results for Foam (b). The full field of the longitudinal strain is considered.

In conclusion, when Foam (a) is used as the core material, particular attention is required for the interface modelling. During the VARTM process, the resin penetrates into the open cells on the foam surface so that the epoxy layer must be included in the modelling in order to accurately predict the structural performance during CSB loading and avoid premature foam crushing under the crack tip. On the other hand, when Foam (b) and Foam (c) are used as core material, the resin layer at the interface is 30 times thinner than for Foam (a) and it can be neglected in the modelling without excessively altering the results. It is worth nothing that during DCB test, the core is not under compression loading and foam crushing does not occur anywhere in the sample. Therefore, including or omitting the resin layer at the interface does not affect the results.

5. Conclusions

This work has investigated the skin-core interfacial behaviour of sandwich structures under Mode I and Mode II loading. Three types of PMI close-celled foam have been used as core material. A weaker surface bonding was found in specimens with a fine-celled foam core, due to the low surface resin uptake. Different values of critical energy release rate were calculated at crack initiation and during propagation for the DCB specimens. The initiation value is related to the fracture toughness of the resin at the interface, while the propagation value is associated with the foam fracture toughness. The crack, in fact, grows inside the foam after the initial micro-kinking phenomenon.

Experimental strain fields, obtained with the DIC technique, are in good agreement with FE predictions when the resin layer at the interface is included in the modelling of CSB specimens. If the resin film is neglected, foam strains are over-predicted, premature crushing under the crack tip occurs and the numerical results are not accurate. However, it is important to note that this is relevant only for coarse-celled foams; omitting the resin layer in the modelling does not significantly affect the results for sandwich samples with fine-celled foam cores.

References

[1] F. Avilés and L. A. Carlsson. Analysis of the sandwich DCB specimen for debond characterization. *Engineering Fracture Mechanics*, 75(2):153-168, 2008.

[2] D. A. Ramantani, M. F. S. F. de Moura, R. D. S. G. Campilho, and A. T. Marques. Fracture characterization of sandwich structures interfaces under mode I loading. *Composites Scence and Technology*, 70(9):1386–1394, 2010.

[3] K. N. Shivakumar and S. a. Smith. In Situ Fracture Toughness Testing of Core Materials in Sandwich Panels. *Journal of Composite Materials*, 38(8):655-668, 2004.

[4] A. A. Saeid and S. L. Donaldson. Experimental and finite element evaluations of debonding in composite sandwich structure with core thickness variations. *Advances in Mechanical Engineering*, 8(9):1-18, 2016.

[5] M. Rinker, M. John, P. C. Zahlen, and R. Schäuble. Face sheet debonding in CFRP/PMI sandwich structures under quasi-static and fatigue loading considering residual thermal stress. *Engineering Fracture Mechanics*, 78(17):2835-2847, 2011.

[6] B. Wang, Y. Shi, C. Zhou, and T. Li. Failure mechanism of PMI foam core sandwich beam in bending. *International Journal for Simulation and Multidisciplinary Design Optimization*, 6(A8), 2015.

[7] J. Wang, H. Wang, X. Chen, and Y. Yu. Experimental and numerical study of the elastic properties of PMI foams. *Journal of Materials Science*, 45(10): 2688–2695, 2010.

[8] L. A. Carlsson and G. A. Kardomateas, *Structural and failure mechanics of sandwich composites*. 2011.

[9] I. Carranza Guisado. Personal communication. 2017.

[10] ASTM D5045-14, "Standard Test Methods for Plane-Strain Fracture Toughness and Strain Energy Release Rate of Plastic Materials 1," *Am. Soc. Test. Mater.*, 99: 1–9, 2014.

[11] ABAQUS User's Manual. ABAQUS Documentation. Dassault Systèmes. 2017.

[12] F. Tufano, D. Roosen, U. Lang, K. Bernhard, and A. Roth. Cost and Weight Reduction of Structureal Sandwich Applications for the Aereospace Industry by the use of a new high performance, high temperature resistant and damage tolerant Core Material. *Proceedings of the SAMPE BRAZIL CONGRESS, São Paulo, Brazil*, November 8, 2016.

[13] J. Scherble and T. Jahn. New Rohacell Development For Resin Infusion Processes. In: *Sandwich Structures 7: Advancing with Sandwich Structures and Materials*, 753–761, 2005

[14] Astm D5528-01. Standard Test Method for Mode I Interlaminar Fracture Toughness of Unidirectional Fiber-Reinforced Polymer Matrix Composites. *Am. Stand. Test. Methods*, 3: 1–12, 2014.